Energy & Environmental Science

PAPER

View Article Online
View Journal | View Issue

Cite this: *Energy Environ. Sci.*, 2014, **7**, 812

Phase diagram of In–Co–Sb system and thermoelectric properties of In-containing skutterudites

Yinglu Tang,†[a] Yuting Qiu,†[bc] Lili Xi,[b] Xun Shi,*[b] Wenqing Zhang,[b] Lidong Chen,[b] Ssu-Ming Tseng,[d] Sinn-wen Chen[d] and G. Jeffrey Snyder*[a]

Received 29th September 2013
Accepted 2nd December 2013

DOI: 10.1039/c3ee43240h

www.rsc.org/ees

In-containing skutterudites have long attracted much attention and debate partly due to the solubility limit issue of indium in $CoSb_3$. The isothermal section of the equilibrium phase diagram for the In–Co–Sb system at 873 K is proposed using knowledge of the related binary phase diagrams and experimental data, which explains the debated indium solubility that depends on Sb content. In this paper, a series of In-containing skutterudite samples ($In_xCo_4Sb_{12-x/3}$ with x varying from 0.075 to 0.6 and $In_{0.3}Co_{4-y}Sb_{11.9+y}$ with y changing from −0.20 to 0.20) are synthesized and characterized. X-ray analysis and scanning electron microscopy images indicate that, up to $x = 0.27$, single-phase skutterudites are obtained with lattice constant increasing with In fraction x. A fixed-composition skutterudite $In_{0.27\pm0.01}Co_4Sb_{11.9}$ was determined for the Co-rich side of In–$CoSb_3$ which is in coexistence with liquid InSb and $CoSb_2$. Indium, like Ga, is expected, from DFT calculations, to form compound defects in In-containing skutterudites. However, relatively higher carrier concentrations of In-containing skutterudites compared to Ga-containing skutterudites indicate the existence of not fully charge-compensated compound defects, which can also be explained by DFT calculations. The net n-type carrier concentration that naturally forms from the complex defects is close to the optimum for thermoelectric performance, enabling a maximum zT of 1.2 for the fixed skutterudite composition $In_{0.27}Co_4Sb_{11.9}$ at 750 K.

Broader context

In-containing skutterudites have long attracted much attention due to the high thermoelectric efficiency and proposed application in automotive waste heat recovery. However there has been much debate over how much indium is actually soluble in $CoSb_3$ or whether it simply precipitates out as nanoparticles. In this study, we provide both theoretical and experimental evidence for the presence of compound defects in skutterudites with indium impurities. The isothermal section of ternary phase diagram of In–Co–Sb system at 873 K is proposed, which naturally explains the solubility debate and the confusion concerning the various reports of maximum solubility of indium in the skutterudite phase. The phase relations allow us to identify a stable skutterudite composition $In_{0.27}Co_4Sb_{11.9}$ with high zT values greater than 1. A wide range of nominal compositions will produce the same skutterudite material as the majority phase which will enable the flexibility needed to produce commercial quantities of reliable, uniform quality.

1. Introduction

Thermoelectric materials have the ability to directly convert heat into electricity. The thermoelectric performance of materials is characterized by the dimensionless figure of merit, $zT = S^2\sigma T/\kappa$ where S is the Seebeck coefficient, σ is the electrical conductivity, T is the absolute temperature, and κ is the total thermal conductivity. By adding filler atoms into the cages, filled skutterudites can have low thermal conductivity like a glass and high electrical conductivity like a crystal, which make them excellent thermoelectric materials according to the "phonon glass electron crystal" (PGEC)[1] concept. Among various kinds of filled skutterudite thermoelectric materials, In-doped skutterudites have attracted much attention. For single filling, zT was reported to achieve 1.2 for $In_{0.25}Co_4Sb_{12}$ at 575 K by He *et al.*[2] For double filling, zT of 1.43 for $In_{0.2}Ce_{0.15}Co_4Sb_{12}$ at 800 K was reported by Li *et al.*[3] However, the nature of In incorporation has not yet been fully understood and there are several different mechanisms for enhancement of zT. One possible mechanism is that the In atom goes into the filler site and due to the rattling and avoided crossing effect,[4] the thermal conductivity becomes greatly decreased, and thus zT is

[a]*Department of Materials Science, California Institute of Technology, Pasadena, California 91125, USA. E-mail: jsnyder@caltech.edu*

[b]*State Key Laboratory of High Performance Ceramics and Superfine Microstructure, Shanghai Institute of Ceramics, Chinese Academy of Sciences, 1295 Dingxi Road, Shanghai 200050, China. E-mail: xshi@mail.sic.ac.cn*

[c]*Graduate University of Chinese Academy of Sciences, Beijing 100049, China*

[d]*Department of Chemical Engineering, National Tsing Hua University, #101, Sec.2, Kuang-Fu Rd., Hsin-Chu 300, Taiwan*

† These authors contributed equally to this work.

enhanced; another possible mechanism is that doping of In results in a nanostructured InSb phase that is evenly distributed on the boundaries of the skutterudite phase,[3] which lowers thermal conductivity and enhances zT. Which mechanism accounts for the good thermoelectric properties of In-doping skuterudites remains unclear. To begin with, there has been much debate about the solubility limit x, of indium in $In_xCo_4Sb_{12}$ where it is typically assumed the In enters into the void filling site.

Theoretically, Shi *et al.*[5] concluded that based on the electronegativity difference between In and Sb, which is less than 0.8, the ideal In-filled materials are thermodynamically unstable. Experimentally, a filling limit of In was first reported to be around $x = 0.22$ in In-doped $CoSb_3$ by He *et al.*[2] and later reproduced by Mallik.[6] In was also observed in the form of secondary phase InSb, and therefore assumed as not entering entirely as filler atoms in $In_xYb_yCo_4Sb_{12}$ with solubility limit of In less than $x = 0.20$ (ref. 7) and in $In_xCe_yCo_4Sb_{12}$ with solubility limit of In less than $x = 0.15$.[3] Recently Sesselmann[8] found that with an indium addition of $x = 0.2$ in $In_xCo_4Sb_{12}$, antimony was found at the grain boundaries of skutterudite phase, which suggests that In substitutes for Sb and adds complexity to the possible position that In atom may go to. Such a substitution was also deduced in the related $Ga_xCo_4Sb_{12-x/3}$ where Ga like In, is a group 13 element in the periodic table. The charge-compensated compound defects (CCCD) recently found in Ga-containing skutterudites $(Ga_{VF})_{2x/3}Co_4Sb_{12-x/3}(Ga_{Sb})_{x/3}$ (ref. 9) demonstrates the possibility that as opposed to normal filled skutterudites with fillers (*e.g.* Na, Ba, Yb) occupying exclusively the voids, In-containing skutterudites may also have such compound defects, meaning that In atom goes to the filler site and Sb site at the same time.

In addition, by studying the phase relations in the In–Co–Sb system Grytsiv[10] identified two solubility limits of indium in $In_xCo_4Sb_{12}$ which depend on the Co/Sb ratio. The maximum solubility $x = 0.22$, which is consistent with Tao He's result, is found when the compound is in equilibrium with $CoSb_2$ and InSb. The solubility of indium in the skutterudite phase is reduced to $x = 0.09$ when it coexists in equilibrium with InSb and (Sb).

In this study, we provide both theoretical and experimental evidence for the presence of compound defects in skutterudites with indium impurities. The isothermal section of ternary phase diagram of In–Co–Sb system at 873 K is proposed, which is based on knowledge of the related binary phase diagrams and the microstructure of samples. The ternary phase diagram naturally explains the solubility debate and the confusion concerning the various reports of maximum solubility of indium in the skutterudite phase. Meanwhile, the complex defects in this system, $(In_{VF})_yCo_4Sb_{12-z}(In_{Sb})_z$ lead to low lattice thermal conductivity.

2. Experimental section

2.1 Sample synthesis

Two sets of samples were prepared by a process of melting followed by high-temperature annealing at 873 K for 7 days. One set is $In_xCo_4Sb_{12-x/3}$ (or equivalently $(In_{VF})_{2x/3}Co_4Sb_{12-x/3}(In_{Sb})_{x/3}$ where In_{VF} and In_{Sb} stand for void-filling, and Sb-substituting In atom respectively) with x changing from 0.075 to 0.60. The other set is $In_{0.3}Co_{4-y}Sb_{11.9+y}$ (equivalently $(In_{VF})_{0.20}Co_{4-y}Sb_{11.9+y}(In_{Sb})_{0.10}$) with y changing from -0.20 to 0.20. High-purity elements Co (99.99%, shot), Sb (99.9999%, piece), and In (99.999%, shot) were used as raw materials. The elements were mixed in Boron Nitride crucibles, and then sealed in fused silica tubes under Ar gas. The silica tubes were heated slowly up to 1353 K, quenched to room temperature, followed by annealing at 873 K for one week. The resulting ingots were ground into fine powders and consolidated by hot pressing at 873 K for 2 h under a pressure of about 60 MPa, yielding fully dense bulk samples. High-density (>95% of the theoretical density of $CoSb_3$) was achieved in all samples.

2.2 Structure characterization

Room temperature powder X-ray diffraction (XRD) data were collected on a D/max 2550V diffractometer equipped with Cu Kα radiation to check phase purity and lattice constant. Quantitative elemental analyses of the annealed samples were performed with a JEOL JXA-8200 electron probe microanalysis (EPMA) using an accelerating voltage of 15KeV and a current of 30 nA in a WDS mode and averaged over 10 randomly selected locations.

2.3 Thermoelectric transport properties

Electrical transport properties, including electrical conductivity (σ) and Seebeck coefficient (S) were measured using the ZEM-3 (ULVAC Co. Ltd.) apparatus under a helium atmosphere from 300 to 800 K. Thermal conductivity (κ) was calculated using the measured thermal diffusivity, specific heat, and sample density. Thermal diffusivity and specific heat were measured in an argon atmosphere using laser flash method (NETZSCH LFA 427) and Shimadzu DSC-50, respectively. The density of the samples was measured using the Archimedes method. Hall coefficients (R_H) were measured in a Quantum-Design Physical Property Measurement System (PPMS) by sweeping the magnetic field up to 3 T in both positive and negative directions. Hall carrier concentration (n) was then estimated to be equal to $1/R_He$, where e is the elementary charge. The Hall carrier mobility (μ_n) was calculated according to the relation $\mu_n = R_H\sigma$.

2.4 First-principles calculations

All the calculations were carried out using the projector augmented wave (PAW) method, as implemented in the Vienna *ab initio* Simulation Package (VASP). The Perdew–Burke–Ernzerhof generalized gradient approximation (GGA) for the exchange-correlation potential was used for all the calculations, and computational details[9] can be found in our earlier publications. All calculations of pure and indium doped $CoSb_3$ skutterudites were carried out on a supercell ($2 \times 2 \times 2$ primitive cell) with a total of 128 atoms and 8 voids. A $3 \times 3 \times 3$ Monkhorst-Pack uniform k-point sampling was used for energy calculations of supercell. Different configuration structures were considered and the one that has the lowest energy was used for further analysis.

3. Results and discussion

3.1 Structural characterizations and phase diagram

Fig. 1 shows the band structures of pure $CoSb_3$, $Co_{32}Sb_{95}In_{Sb}$, $In_{VF}Co_{32}Sb_{95}In_{Sb}$, and $(In_{VF})_2Co_{32}Sb_{95}(In_{Sb})$. Results show that In doping at different sites has different effect on band structures. Pure $CoSb_3$ is a semiconductor with small band gap. One In atom at the Sb substitution site generates a deficiency of two electrons and one In atom at the void-filling position adds one extra electron compared to pure $CoSb_3$. As a result, one In substituting for Sb leads to imbalanced charge and pushes up one Sb-based band above the Fermi level, which brings the system to an unstable state at no charge compensation. For the same reason $In_{VF}Co_{32}Sb_{95}In_{Sb}$ is also hardly stable whereas $(In_{VF})_2Co_{32}Sb_{95}(In_{Sb})$ is charge-balanced and is thus a semiconductor. Intuitively $In_xCo_4Sb_{12-x/3}$, equivalently $(In_{VF})_{2x/3}Co_4Sb_{12-x/3}(In_{Sb})_{x/3}$, is expected to be a stable skutterudite phase.

The charged defects from In-containing $CoSb_3$, such as In_{Co}, In_{Sb} substitutions in the Co–Sb framework, In_{VF} on the crystal void site, and their combinations, with different charge states q are calculated by *ab initio* methods. The defect formation Gibbs free energy per impurity can be written as follows:

$$\Delta G_f(y,w,z,q) = [E_{tot}(In_yCo_{32-w}In_wSb_{96-z}In_{z,q}) - E_{tot}(CoSb_3,bulk) + z\mu_{Sb} + w\mu_{Co} - (y + w + z)\mu In + q(\varepsilon_F + E_V + \Delta V)]/(y + w + z) \quad (1)$$

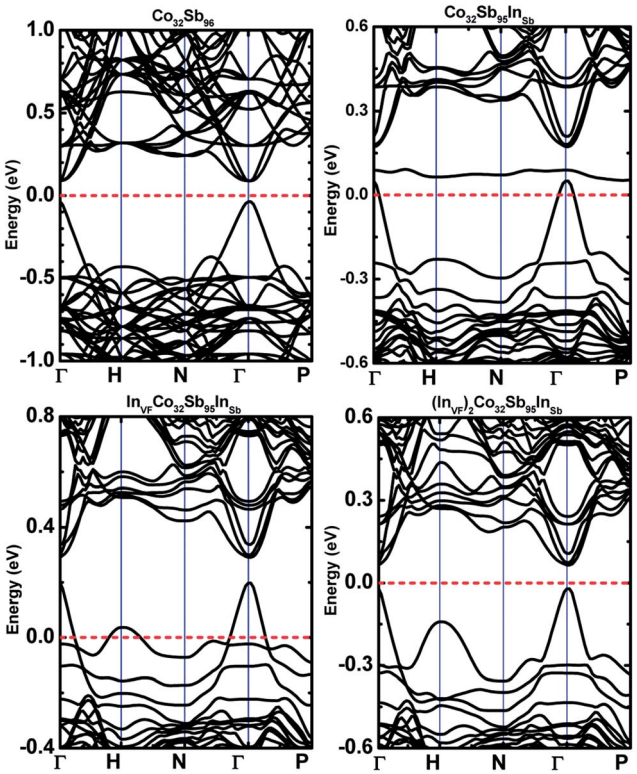

Fig. 1 Band structures of $CoSb_3$ and different In-doped systems. The dashed lines are the Fermi levels.

where $E_{tot}(In_yCo_{32-w}In_wSb_{96-z}In_z,q)$ is the total energy of a 2 × 2 × 2 supercell $In_yCo_{32-w}In_wSb_{96-z}In_z$. $E_{tot}(CoSb_3,bulk)$ is the total energy of supercell of bulk $CoSb_3$. y is the filling fraction of In in crystal voids, w is the substituting fraction at Co sites, and z is the substituting fraction at Sb sites. μ_R is chemical potential for $R_{(R=In,Co,Sb)}$, q is the charge state of the point defect. ε_F is the Fermi level, referring to the valence band maximum E_v in $CoSb_3$. ΔV is the correction term to align the reference potential in the defect supercell with that in the perfect supercell.

Fig. 2 shows the defect formation energy as a function of Fermi level at Co-rich limit, where the system is connected to a Co reservoir. Ga-containing skutterudites form stable charge-compensated compound defects (CCCD) $(Ga_{VF})_{2x/3}Co_4Sb_{12-x/3}(Ga_{Sb})_{x/3}$ when the Fermi level falls in the gap area. The formation energy of the single filling defect $(Ga_{VF})_xCo_4Sb_{12}$ is always very high. In contrast, In-containing skutterudite favors In filling into the void at relatively low Fermi level instead, and dual-site In occupancy can form as the Fermi level increases. In the gap area 0–0.17 eV (shadow in Fig. 2), Ga always forms the charge compensated defect, and In forms either a single filling, or a dual-site defect with or without charge compensation, at different Fermi levels which likely corresponds to different experimental conditions such as the amount of indium impurity or the stoichiometric ratio of Co/Sb.

Fig. 3(a and b) shows the X-ray diffraction results of annealed $In_xCo_4Sb_{12-x/3}$ samples with actual compositions x, as determined from electron probe micro-analysis. All major diffraction peaks are indexable to the skutterudite phase, as identified using JCPDS File no. 65-3144 for $CoSb_3$. However, in samples with the nominal indium content x higher than 0.30 (lower three patterns), small amount of impurity phases (secondary phases other than skutterudite phase), especially InSb and $CoSb_2$, are always observed, which indicates that those samples are outside the single phase region.

Fig. 3(c) plots the dependence of the lattice constant calculated from the XRD data on the actual indium content x. The dependence in the current work agrees with the data of Grytsiv *et al.* As x increases, the lattice constant increases and becomes saturated when nominal $x \geq 0.30$, strongly supporting that the solubility limit of indium is around 0.30.

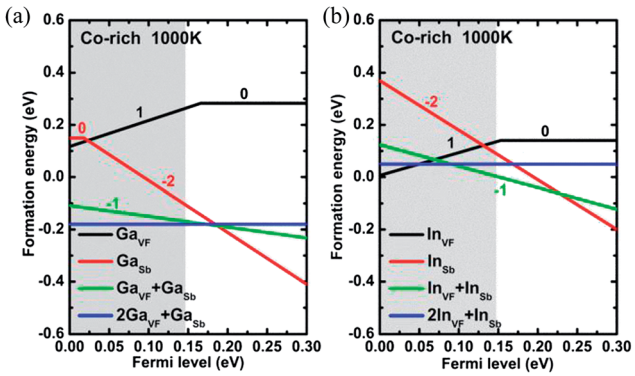

Fig. 2 Formation energies of possible defects as a function of Fermi level at the Co-rich limit in Ga-containing (a) and In-containing (b) skutterudites. The zero Fermi level corresponds to the top of the valence band, and the width of shadowed area indicates the energy gap. The numbers for labelling is the charge state of the point defect.

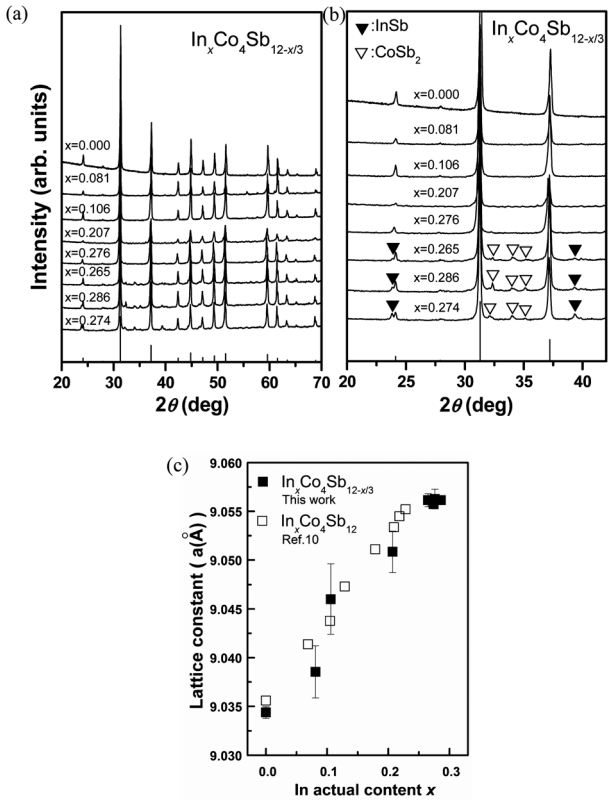

Fig. 3 (a) XRD patterns of the In-containing skutterudites with nominal compositions $In_xCo_4Sb_{12-x/3}$ (x = 0, 0.075, 0.15, 0.225, 0.30, 0.375, 0.45, 0.60) and corresponding actual compositions x = 0, 0.081, 0.106, 0.207, 0.276, 0.265, 0.286, 0.274. (b) Magnification of the XRD patterns. (c) Dependence of lattice constant on actual indium content x. Filled symbols are from this work; open squares denote data from ref. 10.

Table 1 Nominal indium content and total indium content in the skutterudite phase estimated by EPMA for In-containing skutterudites with different compositions. Boldface indium contents correspond to the same skutterudite phase composition $In_{0.27\pm0.01}Co_4Sb_{11.9}$ represented as a magenta circular symbol in Fig. 5b

Samples	Nominal In content	EPMA In content
$In_{0.075}Co_4Sb_{11.975}$	0.075	0.081 ± 0.004
$In_{0.15}Co_4Sb_{11.95}$	0.15	0.106 ± 0.016
$In_{0.225}Co_4Sb_{11.925}$	0.225	0.207 ± 0.013
$In_{0.30}Co_4Sb_{11.90}$	0.30	0.276 ± 0.014
$In_{0.375}Co_4Sb_{11.875}$	0.375	0.265 ± 0.010
$In_{0.45}Co_4Sb_{11.85}$	0.45	0.286 ± 0.012
$In_{0.60}Co_4Sb_{11.80}$	0.60	0.274 ± 0.009
$In_{0.30}Co_{3.8}Sb_{12.1}$	0.30	0.086 ± 0.005
$In_{0.30}Co_{3.9}Sb_{12}$	0.30	0.148 ± 0.011
$In_{0.30}Co_{4.1}Sb_{11.8}$	0.30	0.287 ± 0.020
$In_{0.30}Co_{4.2}Sb_{11.7}$	0.30	0.261 ± 0.012
$In_{0.20}Co_4Sb_{11.8}$	0.20	0.084 ± 0.016
$In_{0.20}Co_4Sb_{12}$	0.20	0.150 ± 0.020

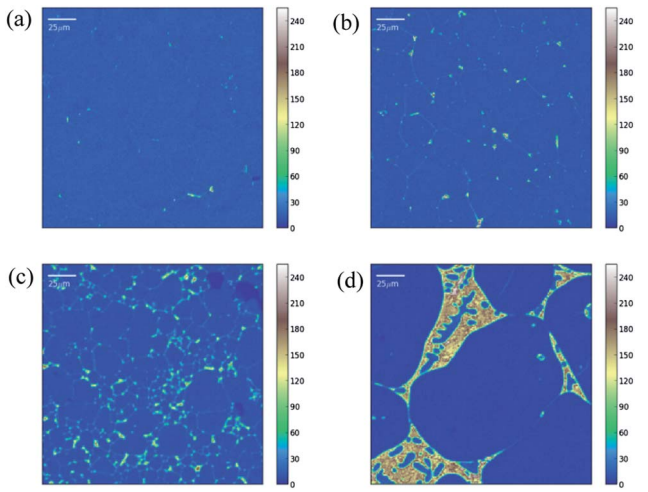

Fig. 4 Electron probe microanalysis (EPMA) indium maps in samples with different nominal compositions. (a) $In_{0.225}Co_4Sb_{11.925}$, (b) $In_{0.30}Co_4Sb_{11.90}$, (c) $In_{0.30}Co_{4.2}Sb_{11.7}$ and (d) $In_{0.30}Co_{3.8}Sb_{12.1}$.

Electron probe microanalysis (EPMA) measurements were carried out at ten different locations on the skutterudite phase region in samples and the average total indium contents are listed in Table 1. The EPMA maps show that there is a significant volume fraction of In-rich impurity phases in the $In_{0.3}Co_{4-y}Sb_{11.9+y}$ samples with compositions that are off the Co/Sb ratio of the CCCD sample $(In_{VF})_{0.20}Co_4Sb_{11.90}(In_{Sb})_{0.10}$ (see Fig. 4c and d). However, in CCCD samples, the indium is nearly completely homogeneously distributed (see Fig. 4a and b) with few secondary phases and the solubility limit of indium is estimated to be around $x = 0.27 \pm 0.01$ according to EPMA data. When the indium amount exceeds 0.27 in CCCD samples, secondary phase such as liquid and $CoSb_2$ is observed in SEM, which is consistent with XRD data presented here. The sensitivity of formation of secondary phases to the ratio of Co/Sb in samples strongly supports the hypothesis that impurity indium atoms form compound defects in $CoSb_3$ by occupying both the void and Sb sites.

The proposed phase diagram of the In-containing skutterudites at 873 K is shown in Fig. 5a, and is based on general knowledge of the binary phase diagrams. The related binary phases of In, Co and Sb are shown on the axes including the known regions of solid or liquid solubility for the binary compounds and a rough estimate of the solubility of the ternary compounds. The exact regions of solid solubility of $CoSb_2$ and $CoSb_3$ are not known but they are enlarged for clarity in Fig. 5a. The white regions of Fig. 5a designate regions which are expected to contain two or three phases in equilibrium at 873 K.

The region near $CoSb_3$ is enlarged in Fig. 5b. Our experimental data suggest that the region of indium solubility extends toward the CCCD samples, $(In_{VF})_{2x/3}Co_4Sb_{12-x/3}(In_{Sb})_{x/3}$, with an estimated maximum x value around 0.27. When x exceeds 0.27, the CCCD samples contain an In-dual-site-doped skutterudite phase with indium doping level around $x = 0.27$ and impurity phases InSb and/or $CoSb_2$. When the nominal composition is off the Co/Sb ratio of CCCD $(In_{VF})_{2x/3}Co_4Sb_{12-x/3}(In_{Sb})_{x/3}$ samples, significant impurity phases form from $x = 0.30$ samples.

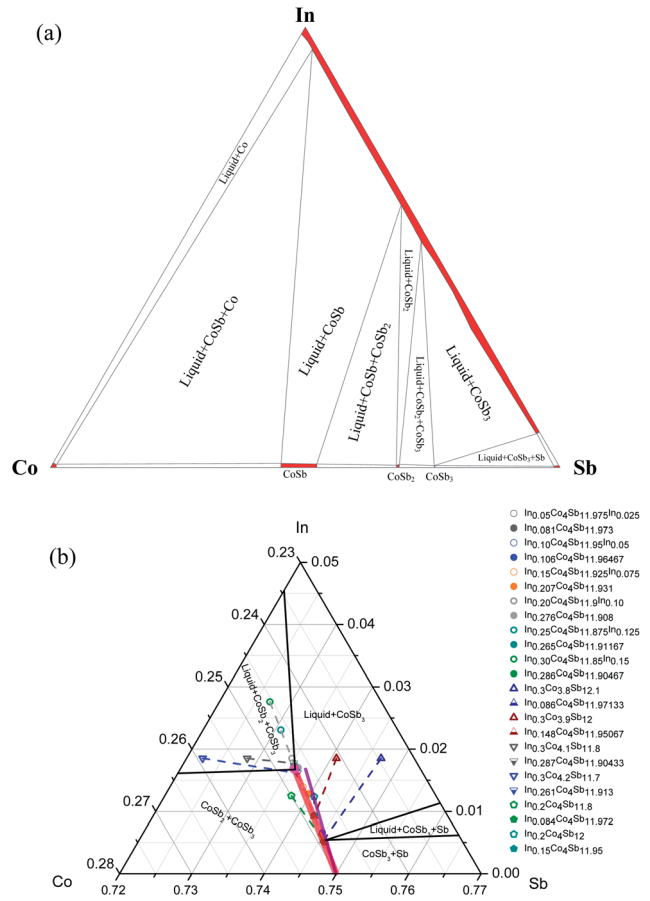

Fig. 5 Proposed phase diagram for In-containing skutterudites at 873 K. (a) Full diagram with related binary phases and approximate regions of solubility indicated by red regions. (b) Phase regions enlarged near $CoSb_3$. Because of the stability of indium in dual sites (CCCD compositions) the region of indium solubility is extended as a red line in the direction of $(In_{VF})_{2x/3}Co_4Sb_{12-x/3}(In_{Sb})_{x/3}$ up to $x = 0.27$. The solid purple line indicates the void filling in the direction $(In_{VF})_xCo_4Sb_{12}$ up to $x = 0.27$. The magenta circular symbol represents the composition of skutterudite phase $In_{0.27}Co_4Sb_{11.9}$ obtained when the nominal composition is in the three phase region (liquid, $CoSb_2$ and In–$CoSb_3$). The nominal sample compositions are shown as open symbols. Solid symbols represent the composition of the skutterudite majority phase using the experimental EPMA value for indium content which is below 0.27 for all samples, and positioned on the red CCCD line. The nominal (open symbols) and experimental compositions (solid symbols) are connected with a dotted line. The samples with nominal CCCD compositions when $x < 0.30$ appear to be within the solubility limit, the closed symbols of which are shifted away from the red solubility line according to the observed carrier concentration as explained in Section 3.2.4.

When the nominal composition is slightly Sb-rich ($In_{0.3}Co_{4-y}Sb_{11.9+y}$, $y > 0$), the nominal composition is in a two-phase region between In–$CoSb_3$ and liquid In–Sb where both phases have variable indium content in this region. According to the phase rule, the degrees of freedom $F = C - P + 0 = 3-2 = 1$ where C means the number of components and P means the number of phases, 0 indicates both temperature and pressure are fixed. Thus this two-phase region has an additional degree of freedom to describe the tie line between which phases with variable In content form. We observe that the tie line connecting the nominal composition and the skutterudite phase is quite steep, which leads to a much lower In content in the skutterudite phase with an In-rich liquid In–Sb impurity phase. It is reasonable that In prefers the high entropy of the liquid rather than the solid skutterudite phase.

In contrast to the Sb rich side, when the nominal composition is slightly Co-rich ($In_{0.3}Co_{4-y}Sb_{11.9+y}$, $y < 0$), it is in a three phase region between three phases with fixed compositions, approximately liquid InSb, $In_{0.27}Co_4Sb_{11.9}$ and $CoSb_2$. The compositions in a three phase region are fixed because of the phase rule, $F = C - P + 0 = 3-3 = 0$. The composition of the liquid InSb ($In_{0.53}Sb_{0.47}$) is fixed near the composition of the InSb phase which is stable up to 798.7 K. Because the phase boundary between two phase region and three phase region must be a straight line, the point of contact (magenta circular symbol) between the skutterudite phase and the phase triangle must have relatively high indium content. Because of the phase rule all the compositions in this three phase region will produce the same skutterudite composition with high actual indium content ($In_{0.27}Co_4Sb_{11.9}$). This was confirmed by the EPMA measurements to be $x = 0.27 \pm 0.01$ as shown in Table 1.

The steep slope of the tie line on the Sb-rich side of the stable phase (two phase region: liquid and $CoSb_3$) results in relatively lower In content in the skutterudite phase, when compared to the fixed composition $In_{0.27}Co_4Sb_{11.9}$ obtained from samples with nominal compositions on the Co-rich side with sufficient indium content (three phase region: liquid, $CoSb_2$, and $CoSb_3$). This indicates that being slightly Co-rich instead of Sb-rich is more favorable in order to achieve high indium content in the skutterudite phase. Moreover, it also sheds light on why there is a solubility difference when the skutterudite phase is in coexistence with different impurity phases.[10] As the phase width appears to be quite narrow, small variations of composition will lead to different two or three phase equilibrium regions on the phase diagram which can explain why different attempts to produce the same material may in fact produce very different skutterudite materials with different filling fraction, and therefore different thermoelectric properties. In addition the Co-rich and Sb-rich sides of the single phase region (red line in Fig. 5b) will have different temperature dependent characteristics and could lead to different precipitation products as found in Zn–Sb.[11] For example solid solubility is typically temperature dependent and can be used to form nano-scale coherent precipitates,[12] which may explain the observance of InSb in some samples[3,7,13] but not others.[14–17]

3.2 Thermoelectric properties

3.2.1 Electrical transport. The temperature dependence of the Seebeck coefficients and electrical conductivities of $In_xCo_4Sb_{12-x/3}$ (EPMA determined x = 0.081, 0.106, 0.207, 0.276) is shown in Fig. 6a and b, respectively. All the samples show negative Seebeck coefficients throughout the whole temperature range, indicating n-type semiconductor behavior. With increasing temperature, the magnitude of the Seebeck coefficient increases first and starts decreasing after reaching a

peak, which is possibly induced by the bipolar effect. Meanwhile, the electrical conductivity (Fig. 6b) decreases smoothly as temperature increases. As In content increases, the electrical conductivity increases and the magnitude of Seebeck coefficient decreases, which suggests that some of the indium acts as an n-type dopant to increase the carrier concentration.

Intrinsic $CoSb_3$ is a valence precise semiconductor where the doping effect of defects can be understood with Zintl chemistry.[18] Ga-containing $CoSb_3$ skutterudites $(Ga_{VF})_{2x/3}Co_4Sb_{12-x/3}(Ga_{Sb})_{x/3}$ form charge-compensated compound defects which also makes them valence precise semiconductors. An indium atom at the void filling site (In_{VF}) shows an effective charge state +1 and contributes one extra electron to the doped system. Indium atoms at the Sb-substitutional site accept two electrons. Thus, $(In_{VF})_{2x/3}Co_4Sb_{12-x/3}(In_{Sb})_{x/3}$ should also be a valence precise semiconductor as demonstrated in Fig. 1d.

However, the relatively high electron concentrations (as measured by Hall effect) and their dependence in the In-containing $CoSb_3$ samples compared to Ga-containing $CoSb_3$ samples suggests that the indium defects are not entirely charge compensated, with some excess indium as electron donor defects most likely In_{VF} (Fig. 7a). Indeed Fig. 2 predicts that one electron donor defects from In_{VF} are low energy defects particularly at low Fermi levels. Detailed calculations of all defects are necessary for quantitative discussion[19] and will be described in detail elsewhere.[20]

The mixed defect types (complex compound defects) may also lead to a slight change of the direction of the single phase region (red line) in Fig. 5b. For excess indium donor defects in the void filling site, the single phase region would move toward the purple line ($In_xCo_4Sb_{12}$).

As shown in Fig. 7b the *S*–*n* dependence in indium-containing complex compound defect samples follows the extrapolated curve of normal filled skutterudites[2,5,21–28]. Fig. 7b further indicates that due to the In or Ga-rich secondary phases on the grain boundary (as observed in SEM), the $G_xCo_4Sb_{12}$ (G = In, or Ga) samples have very low electron concentrations and large thermopowers from low G content in the skutterudite phase.[29,30] That all the data fall on the same curve in Fig. 7b also provides strong evidence that the band structure in In-containing skutterudites is virtually unchanged near the Fermi level because the same trend is observed in the normally filled as well as in the Ga-containing skutterudites. This is fully consistent with our band structure calculations shown in Fig. 1 and discussions in Section 3.2.1.

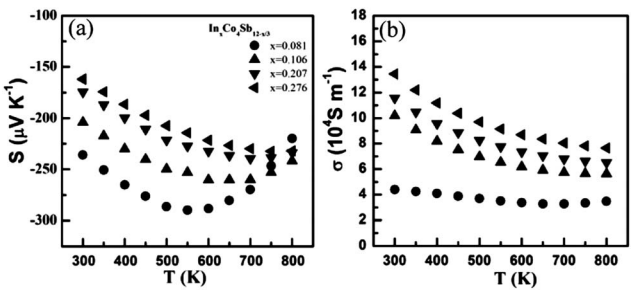

Fig. 6 Temperature dependence of the thermopower (*S*) and electrical conductivity (σ) for samples of $In_xCo_4Sb_{12-x/3}$ with different indium impurity content.

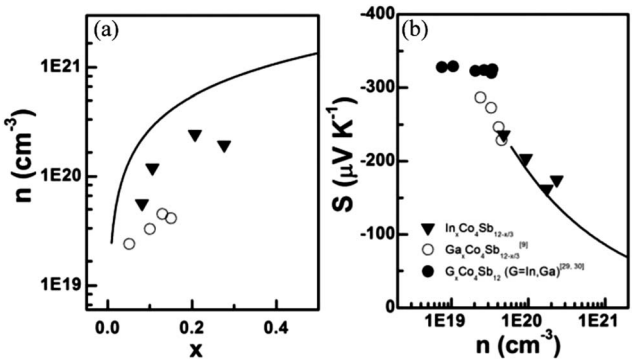

Fig. 7 (a) Room temperature electron concentration (*n*) as a function of indium impurity fraction *x* in In-containing complex compound defect (CCD) skutterudites. The solid line represents the theoretical curve calculated by using $n = 2x/a^3$ where *a* is the lattice constant of $CoSb_3$. (b) Room temperature *S* as a function of electron concentration for In-containing CCD skutterudites at 300 K. The *x* values are estimated by EPMA for CCD samples and CCCD samples from ref. 9 while they are the nominal values for the single-type defect samples from ref. 29 and 30. The solid line represents the general trend for single filled-$CoSb_3$ with those typical electropositive filler species taken from ref. 2, 5 and 21–28.

3.2.2 Thermal transport. Fig. 8 shows the temperature dependence of total thermal conductivity (κ) of the samples $(In_{VF})_{2x/3}Co_4Sb_{12-x/3}(In_{Sb})_{x/3}$ with nominal charge-compensated compound defects. In the whole temperature range investigated, the total thermal conductivity for all samples are lower than 3.5 W m^{-1} K^{-1}. As usual, κ_L is obtained by subtracting the electronic contribution from the total thermal conductivity using the Wiedemann–Franz law. We adopted a Lorentz number of 2.0×10^{-8} V^2 K^{-2} to simplify the estimation of electronic thermal conductivity, and this value is also consistent with the experimentally estimated value based on our previous

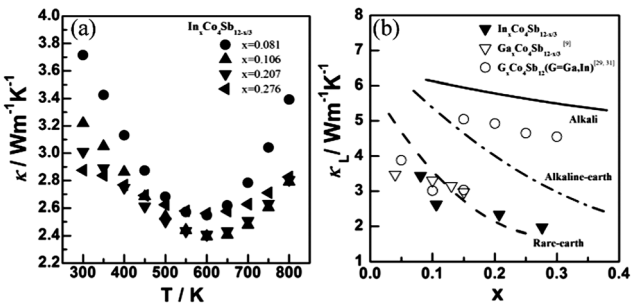

Fig. 8 (a) Temperature dependence of total thermal conductivity and (b) Room-temperature lattice thermal conductivity as a function of the indium impurity fraction in skutterudites. The κ_L trends for alkaline (solid line), alkaline-earth (dashed-dotted line), and rare-earth (dashed line) fillings are shown for comparison. The black triangles are for the indium-containing skutterudites with complex compound defects in the present work. The blank triangles are for Ga-containing skutterudites with charge-compensated compound defects.[9] And the blank circles are for the group 13 element-doped skutterudites[29,31] using the as-reported compositions, presumably assumed to form a single-type defect.

work on skutterudites taken from ref. 22. All In-containing samples present strongly reduced κ_L as compared to binary $CoSb_3$ with $\kappa_L \sim 10$ W m^{-1} K^{-1} at 300 K. Compared with the observed dependence of κ_L on impurity filling fraction in the normal alkaline- or alkaline-earth-filled $CoSb_3$, κ_L reduction in the In-containing samples has a strong dependence on impurity content, as shown in Fig. 8b. At In content as low as 0.106, κ_L could be reduced to 2.62 W m^{-1} K^{-1}, which is even lower than that for $Ga_xCo_4Sb_{12-x/3}$ ($x = 0.15$). Interestingly, the lattice thermal conductivity for the In-containing systems is close to the κ_L for the normal rare earth-filled $CoSb_3$.

The dramatic reduction of lattice thermal conductivity in samples with complex compound defects could perhaps be explained by the dual-site occupation of indium impurities and therefore a dual-character phonon scattering mechanism. The indium impurity at the Sb-substitutional site establishes a point defect with size and bonding (in addition to slight mass) mismatch from the host Sb atoms, leading to the scattering of high-frequency lattice phonons. The indium atoms at the void sites behave as a typical filler species and scatter long wavelength phonons *via* resonant scattering and avoided crossing mechanisms. Therefore, the effective reduction of κ_L implies that a broad spectrum of lattice phonons could be scattered in the In-containing skutterudites with a complex compound defect. The relatively high indium doping content, when counting indium impurities at both the void and Sb sites, is important as it controls the magnitude of the phonon scattering effect.

3.2.3 Thermoelectric figure of merit. Fig. 9 shows the temperature dependence of dimensionless thermoelectric figure of merit (zT) which are consistent with prior reports from ref. 31. The maximum zT value in $In_xCo_4Sb_{12-x/3}$ samples reaches 1.2 (at 750 K) with indium content $x = 0.276$. The complex compound defect containing $In_xCo_4Sb_{12-x/3}$ samples presented in this work are also stable and have good repeatability of thermoelectric properties during the measurements, as shown in Fig. 10.

3.2.4 Not fully charge-compensated compound defects. Compared with $(Ga_{VF})_{2x/3}Co_4Sb_{12-x/3}(Ga_{Sb})_{x/3}$ samples, the compound defect samples of the indium system have relatively larger carrier concentrations, which may be due to the defects not being fully charge-compensated as discussed in Section 3.2.1. If

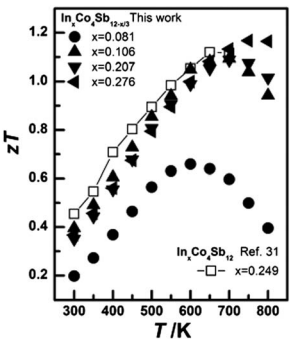

Fig. 9 Temperature dependence of thermoelectric figure of merit (zT) for In-containing skutterudites with complex compound defect (CCD). The x values are the same as the ones in Fig. 6 and 8.

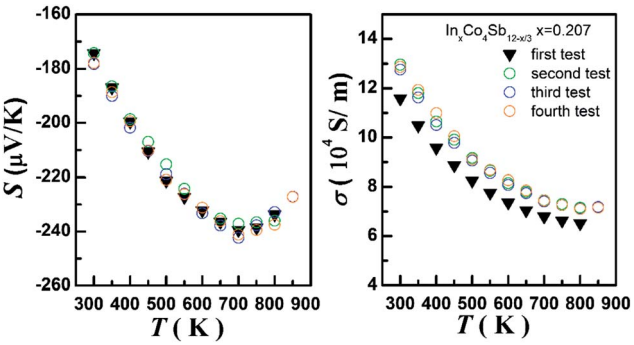

Fig. 10 Repeatability of thermoelectric properties of In-containing skutterudite with complex compound defect (CCD) and $x = 0.207$.

Table 2 Not fully charge-compensated compound defect samples $(In_{VF})_{(2x+\delta)/3}Co_4Sb_{12-(x-\delta)/3}(In_{Sb})_{(x-\delta)/3}$

Samples	n_H (10^{20} cm^{-3})	δ	x	$(2x + \delta)/3$
$In_{0.075}Co_4Sb_{11.975}$	0.48	0.013	0.081	0.058
$In_{0.15}Co_4Sb_{11.95}$	0.93	0.026	0.106	0.079
$In_{0.225}Co_4Sb_{11.925}$	2.35	0.065	0.207	0.160
$In_{0.30}Co_4Sb_{11.9}$	1.74	0.048	0.276	0.200

we write the compositions in a way containing both single filling defects ($(In_{VF})_\delta$) and dual-site compound defects ($(In_{VF})_{2(x-\delta)/3}$ and $(In_{Sb})_{(x-\delta)/3}$), such as $(In_{VF})_{(2x+\delta)/3}Co_4Sb_{12-(x-\delta)/3}(In_{Sb})_{(x-\delta)/3}$, where δ can be calculated using the measured Hall carrier concentration n_H and lattice constant a:

$n_H = \frac{2\delta}{a^3}$, then we can get the value of filling fraction $(2x + \delta)/3$ with x being the content of indium determined by EPMA, as shown in Table 2.

If we plot the compositions $(In_{VF})_{(2x+\delta)/3}Co_4Sb_{12-(x-\delta)/3}(In_{Sb})_{(x-\delta)/3}$ obtained in Table 2 in the enlarged ternary phase diagram in Fig. 5b, we can see that the maximal solubility line will slightly change its direction to somewhere between the direction of $(In_{VF})_{2x/3}Co_4Sb_{12-x/3}(In_{Sb})_{x/3}$ – $CoSb_3$ and the direction of $(In_{VF})_xCo_4Sb_{12}$ – $CoSb_3$, which corresponds to a certain thickness of the solubility region and a ratio of void-filling/Sb-substituting of indium larger than two (with complete charge compensation this ratio is two).

Conclusions

Two sets of samples were prepared by a process of melting followed by long-term high-temperature annealing, $(In_{VF})_{2x/3}Co_4Sb_{12-x/3}(In_{Sb})_{x/3}$ with x changing from 0.075 to 0.30 and $In_{0.30}Co_{4-y}Sb_{11.9+y}$ with y changing from −0.20 to 0.20. XRD and EPMA analysis indicate that when x is less than 0.27, pure single phase skutterudites can be obtained, whereas if x is larger than 0.27 or the composition is off the direction of $(In_{VF})_{2x/3}Co_4Sb_{12-x/3}(In_{Sb})_{x/3}$ then secondary phases start to form. The maximum indium solubility limit is experimentally confirmed to be around $x = 0.27$.

Thermoelectric properties were measured and a maximal zT value of 1.2 was obtained at 750 K when $x = 0.27$. The relatively larger carrier concentrations compared to Ga-containing skutterudites indicate the possibility of not fully charge-compensated compound defects, meaning single filling defects may coexist with dual-site compound defects, which may slightly change the direction along which the solubility region is aligned.

Acknowledgements

This work is partially supported by National Basic Research Program of China (973-program) under Project no. 2013CB632501, National Natural Science of Foundation of China (NSFC) under the no. 11234012, 51121064, and 51222209. The authors acknowledge the financial support of National Science Council of Taiwan (NSC101-3113-P-008-001).

Notes and references

1 G. A. Slack, in *CRC Handbook of Thermoelectrics*, ed. D. M. Rowe, CRC Press, 1995, pp. 407–440.
2 T. He, J. Z. Chen, H. D. Rosenfeld and M. A. Subramanian, *Chem. Mater.*, 2006, **18**, 759–762.
3 H. Li, X. Tang, Q. Zhang and C. Uher, *Appl. Phys. Lett.*, 2009, **94**, 102114.
4 M. Christensen, A. B. Abrahamsen, N. B. Christensen, F. Juranyi, N. H. Andersen, K. Lefmann, J. Andreasson, C. R. Bahl and B. B. Iversen, *Nat. Mater.*, 2008, **7**, 811–815.
5 X. Shi, S. Bai, L. Xi, J. Yang, W. Zhang, L. Chen and J. Yang, *J. Mater. Res.*, 2011, **26**, 1745–1754.
6 R. C. Mallik, C. Stiewe, G. Karpinski, R. Hassdorf and E. Müller, *J. Electron. Mater.*, 2009, **38**, 1337–1343.
7 J. Graff, S. Zhu, T. Holgate, J. Peng, J. He and T. M. Tritt, *J. Electron. Mater.*, 2011, **40**, 696–701.
8 A. Sesselmann, T. Dasgupta, K. Kelm, E. Müller, S. Perlt and S. Zastrow, *J. Mater. Res.*, 2011, **26**, 1820–1826.
9 Y. T. Qiu, L. L. Xi, X. Shi, P. F. Qiu, W. Q. Zhang, L. D. Chen, J. R. Salvador, J. Y. Cho, J. H. Yang, Y. C. Chien, S. W. Chen, Y. L. Tang and G. J. Snyder, *Adv. Funct. Mater.*, 2013, **23**, 3194–3203.
10 A. Grytsiv, P. Rogl, H. Michor, E. Bauer and G. Giester, *J. Electron. Mater.*, 2013, **42**, 2940–2952.
11 G. S. Pomrehn, E. S. Toberer, G. J. Snyder and A. van de Walle, *Phys. Rev. B: Condens. Matter Mater. Phys.*, 2011, 83.
12 T. Ikeda, V. Ravi and G. Snyder, *Acta Mater.*, 2009, **57**, 666–672.
13 S. Ballikaya, G. Wang, K. Sun and C. Uher, *J. Electron. Mater.*, 2010, **40**, 570–576.
14 J. Y. Peng, P. N. Alboni, J. He, B. Zhang, Z. Su, T. Holgate, N. Gothard and T. M. Tritt, *J. Appl. Phys.*, 2008, **104**, 053710.
15 J. Peng, J. He, Z. Su, P. N. Alboni, S. Zhu and T. M. Tritt, *J. Appl. Phys.*, 2009, **105**, 084907.
16 W. Y. Zhao, C. L. Dong, P. Wei, W. Guan, L. S. Liu, P. C. Zhai, X. F. Tang and Q. J. Zhang, *J. Appl. Phys.*, 2007, **102**, 113708.
17 W. Y. Zhao, P. Wei, Q. J. Zhang, C. L. Dong, L. S. Liu and X. F. Tang, *J. Am. Chem. Soc.*, 2009, **131**, 3713–3720.
18 E. S. Toberer, A. F. May and G. J. Snyder, *Chem. Mater.*, 2010, **22**, 624–634.
19 G. S. Pomrehn, A. Zevalkink, W. G. Zeier, A. van de Walle and G. J. Snyder, in preparation.
20 L. Xi and W. Zhang, in preparation.
21 Y. Z. Pei, J. Yang, L. D. Chen, W. Zhang, J. R. Salvador and J. Yang, *Appl. Phys. Lett.*, 2009, **95**, 042101.
22 X. Shi, J. Yang, J. R. Salvador, M. Chi, J. Y. Cho, H. Wang, S. Bai, W. Zhang and L. Chen, *J. Am. Chem. Soc.*, 2011, **133**, 7837–7846.
23 X. Shi, H. Kong, C. P. Li, C. Uher, J. Yang, J. R. Salvador, H. Wang, L. Chen and W. Zhang, *Appl. Phys. Lett.*, 2008, **92**, 182101.
24 S. Q. Bai, Y. Z. Pei, L. D. Chen, W. Q. Zhang, X. Y. Zhao and J. Yang, *Acta Mater.*, 2009, **57**, 3135–3139.
25 Y. Z. Pei, L. D. Chen, W. Zhang, X. Shi, S. Q. Bai, X. Y. Zhao, Z. G. Mei and X. Y. Li, *Appl. Phys. Lett.*, 2006, **89**, 221107.
26 L. D. Chen, T. Kawahara, X. F. Tang, T. Goto, T. Hirai, J. S. Dyck, W. Chen and C. Uher, *J. Appl. Phys.*, 2001, **90**, 1864.
27 J. S. Dyck, W. Chen, C. Uher, L. Chen, X. Tang and T. Hirai, *J. Appl. Phys.*, 2002, **91**, 3698.
28 G. S. Nolas, M. Kaeser, R. T. Littleton and T. M. Tritt, *Appl. Phys. Lett.*, 2000, **77**, 1855.
29 A. Harnwunggmoung, K. Kurosaki, T. Plirdpring, T. Sugahara, Y. Ohishi, H. Muta and S. Yamanaka, *J. Appl. Phys.*, 2011, **110**, 013521.
30 Y. Du, K. F. Cai, S. Chen, Z. Qin and S. Z. Shen, *J. Electron. Mater.*, 2011, **40**, 1215–1220.
31 R. C. Mallik, *Met. Mater. Int.*, 2008, **14**, 223–228.